



## Seismic performance of the Accordion-Web RBS connection

Seyed Rasoul Mirghaderi, Shahabeddin Torabian\*, Ali Imanpour

School of Civil Engineering, University of Tehran, P.O. Box 11365-4563, Tehran, Iran

### ARTICLE INFO

#### Article history:

Received 13 November 2008

Accepted 19 September 2009

#### Keywords:

RBS connection  
Corrugated web  
Cyclic loading  
Special moment frame  
Accordion effect  
Inelastic rotation

### ABSTRACT

A new type of Reduced Beam Section (RBS) connection, “Accordion Web RBS (AW-RBS)”, is presented in this research. RBS connections are commonly known as connections with reduced flange width within a limited area near the column face. However, the AW-RBS decreases the web contribution in moment strength and a reduced section is developed in the beam. In an AW-RBS, the flat web is replaced by corrugated plates (L-shape folded plates, used here) at the expected location of the beam’s plastic hinge. While the corrugated web has adequate shear strength, its provided moment strength and flexural stiffness are negligible. Two relatively identical specimens including AW-RBS connections have been tested under cyclic loading. Both specimens provide at least 8% story drift, without any significant strength loss, which is more than current requirements for qualifying connections in special moment frames. The accordion effect of the corrugated web and the cyclic performance of the connection are verified by analytical results. According to the analytical and experimental results, the inelastic rotations of the connection are mostly provided by reliable and ductile rotation at the reduced region rather than in the connection plates or panel zone.

© 2009 Elsevier Ltd. All rights reserved.

### 1. Introduction

Reduced Beam Section (RBS) moment connection is one of the most economical and practical prequalified connections among the post-Northridge ones. RBS connections were developed on the basis of a new concept named “Weakening”. By this concept, the flexural strength of the beam is reduced in the vicinity of the column face, compared to other nearby sections, by beam section reduction, and this forces a plastic hinge to be formed at the reduced location. The localization of the plastic hinge reduces the fracture vulnerability of beam-to-column complete joint penetration (CJP) welds, and therefore the connection inelastic deformation capacity is improved. A conventional type of RBS moment connection was developed by flange shaving and is known as a “Dogbone” connection; it was first developed during a research project. The project was sponsored by Arbed (a Luxembourg based steel producer) on the basis of Plumier’s idea [1] in order to provide energy dissipative zones for structures. However, the connection was not commonly used until SAC programs for reduction of earthquake hazards in steel moment frame structures.

SAC has reported the results of 45 well-documented RBS connection tests, conducted after the Northridge earthquake [2]. The main variables in these tests were the shape of flange cut (straight cut, tapered cut or radius cut), depths of columns and

beams and web connection. According to the results, the radius cut RBS connection showed successful behavior; the connection behavior depended on the beam depth; bolted and welded web connections had relatively similar behaviors. The SAC Phase II program, including 17 large-scale tests, was planned in order to improve the performance and reduce the economical costs of RBS connections [2]. The main achievement of these tests related to the assessment of beam instabilities such as web and flange local buckling and subsequent lateral–torsional buckling. Such instabilities cause degradation in the connection strength at large rotation demands.

In addition to SAC programs, other investigations were followed on conventional RBS connection. Chi and Uang et al. [3,4] studied experimentally the cyclic behavior of RBS moment connections with deep wide-flange column sections and proposed a seismic design procedure. In similar research, the seismic behavior of RBS moment connections to deep wide-flange columns was studied by Zhang and Ricles [5,6] with regard to the composite floor slab effect. The effect of panel zone strength and beam web connection method on the seismic performance of RBS connections was widely investigated by Lee et al. [7]. These results showed poor behavior of a bolted web connection compared to a welded one. Meanwhile, a criterion was proposed to achieve a balance panel zone that increases the plastic hinge rotation capacity. Nakashima [8] et al. studied analytically and numerically the lateral–torsional instability and lateral bracing effects of wide-flange steel beams subjected to cyclic loading. Furthermore, a statistical study, addressing the cyclic instability of steel moment connections with reduced beam section, was presented by Uang and Fan [9]. Shen

\* Corresponding author. Tel.: +98 21 4405 3876; fax: +98 21 8874 1819.

E-mail addresses: [smirghaderi@ut.ac.ir](mailto:smirghaderi@ut.ac.ir) (S.R. Mirghaderi), [torabian@ut.ac.ir](mailto:torabian@ut.ac.ir) (S. Torabian), [aimanpour@gmail.com](mailto:aimanpour@gmail.com) (A. Imanpour).

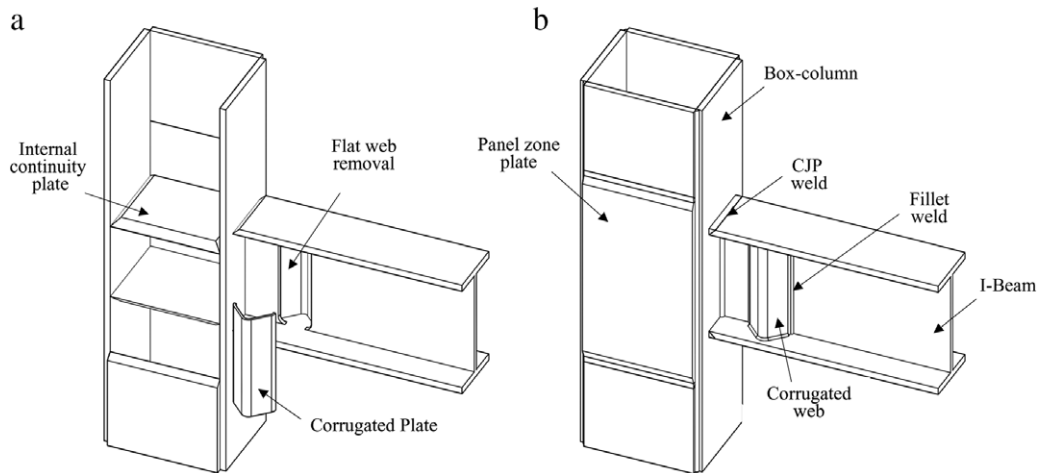


Fig. 1. Proposed connection: (a) Assembly; (b) Configuration.

et al. [10], Kitjasetanphun et al. [11] and Jin and El-Tawil [12] conducted analytical studies on the seismic performance of steel moment-resisting frames including RBS connections. The results confirmed that RBS frames can economically provide proper seismic performance in regions of high seismic risk.

Other than “Dogbone” connections, a few reducing details have been proposed for RBS connections, some of which are as follows:

1. Drilling a set of holes on the beam flanges to reduce the flange contribution to the beam moment capacity [1,13].
2. Making large holes in the beam web to eliminate the web contribution in the moment. The detail was named Reduced Web Connection [14].
3. Reducing the beam web depth in a limited region to decrease the distance between flanges and, consequently, reduce the beam flexural strength. The formed connection was named a wedge detail [15].

Scientifically parallel to the above-mentioned innovative RBS connections, a new RBS connection is presented for steel moment-resisting frames in this paper. In the proposed connection, the beam section is reduced using corrugated plates instead of a flat web at the expected location of the beam’s plastic hinge in the vicinity of the beam-to-column connection. Here, a design procedure is developed for the proposed connection based on the expected behavior of a plastic hinge with a corrugated web as well as general recommendations of AISC seismic provision [16]. Furthermore, an experimental program is conducted on two relatively identical designed specimens in order to investigate the seismic behavior and cyclic response of the new proposed connection. In this regard, the connection is studied analytically to verify the performance of the proposed connection and for profound insight into its seismic behavior.

## 2. The proposed connection: AW-RBS

The assembly and configuration of the proposed connection are illustrated in Fig. 1. As shown in the figure, the web of a beam, with I-section, is removed in a limited zone near the column face and replaced by corrugated plates; in particular, two L-shape folded plates are employed in this study. The beam is connected to the column face by CJP welds to develop a full capacity rigid connection. Based on the accordion behavior of a corrugated web, the contribution of the beam web is expected to be negligible in the beam bending moment strength within the corrugated region. Therefore, a reduced section is formed and the corrugated web can be designed to provide adequate shear capacity.

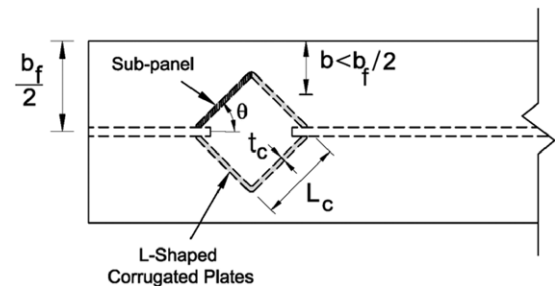


Fig. 2. Unrestrained width of beam flange in the corrugated region of the proposed connection.

A limited region of reduced section in the vicinity of CJP welds reduces the demands of the plastic hinge. This fact conforms exactly to the weakening concept. The connection proposed in this research is supposed to be in the reduced connection category. This RBS connection is called “Accordion-Web RBS connection”, abbreviated as “AW-RBS”.

In this connection, the corrugated web in the plastic hinge region improves the web stability condition due to the larger out-of-plane stiffness of the corrugated web about the beam’s longitudinal axis, and also the flange stability condition due to the smaller width to thickness ratio of beam flange, as shown in Fig. 2. Moreover, it can be expected that all inherent characteristics of corrugated web beams are applicable in the reduced region.

In corrugated web beams, applications of thin plates are allowed without needing vertical stiffeners because of the corrugated webs. Therefore, the cost of beam fabrication is considerably reduced and its fatigue life is improved. There are many researches on various aspects of corrugated web beams and the following significant results are listed as follows [17–19]:

- Due to the “accordion effect” of the web resulting from its low axial stiffness in stretching and contracting, the corrugated web offers a negligible contribution to the moment carrying capacity of the beam. The ultimate beam moment capacity will be based only on the flange yield stress.
- There is no interaction between flexural and shear behavior of beams with a corrugated steel web. The web solely provides the shear strength, which is controlled by three modes of buckling: local buckling mode, global buckling mode and interaction mode.
- The fatigue life of plate girders with corrugated webs is about 40% (average) higher than that of conventionally stiffened plate girders with a stiffener cut short by about four times the web thickness from the tension flange.

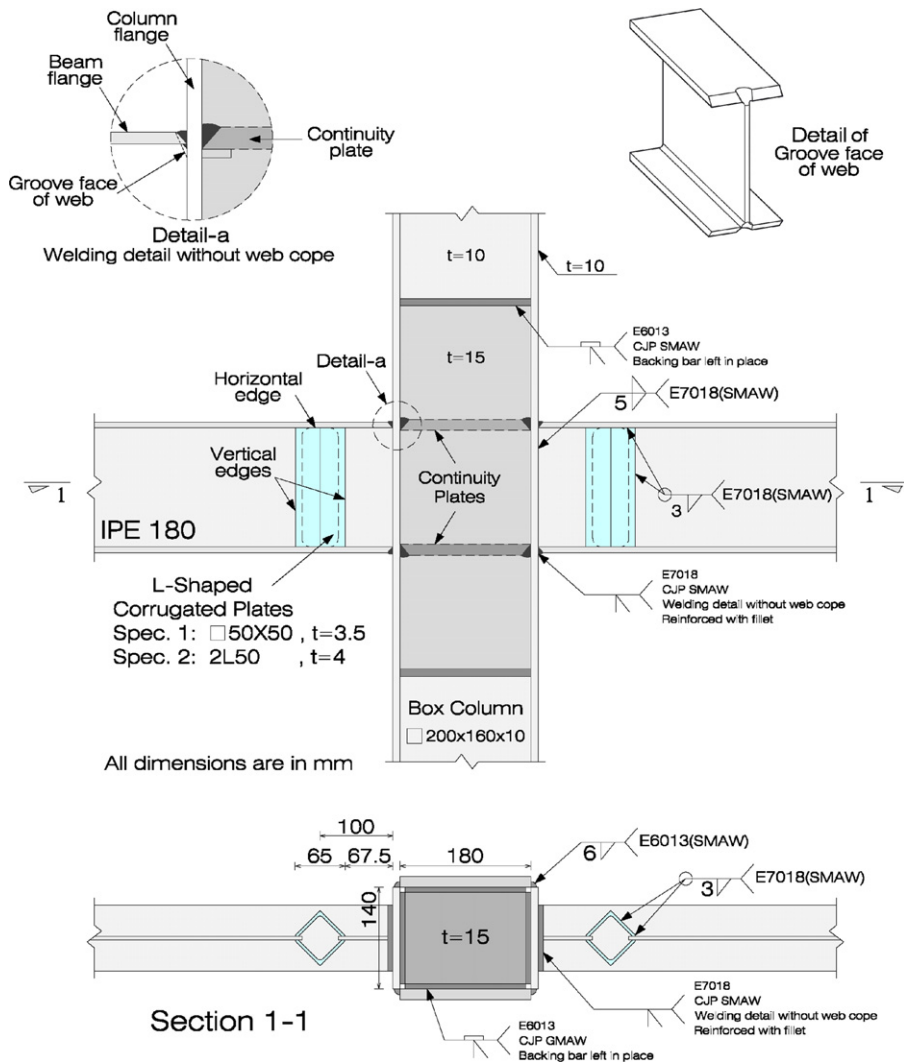


Fig. 3. Test Specimens 1 and 2 connection details.

- The resistance of girders with a corrugated web to the lateral torsion–flexure buckling is about 25% (average) higher compared to that of plate girders with traditional plane webs to lateral buckling.

Regarding the foregoing features, it is expected that the stability and ductility of the beam are improved within the plastic hinge region, and therefore an acceptable seismic behavior is achieved. However, this has to be tested, because the proposed connection locally replaces the web with a double accordion, creating a vertical closed section, which might be less flexible than a classical accordion web.

### 3. Experimental program

The behavior of connections, under cyclic loading, cannot be reliably predicted only by analytical means. Therefore, a set of experimental tests has been carried out to study the behavior of AW-RBS moment connections and to reveal potential problems as well as to verify the analytical results.

#### 3.1. Test specimens

In this research two 2/3 scale specimens, almost identical, including accordion web RBS connections, were designed to be

tested. The specimens consisted of cruciform interior connection subassemblies with beams attached to the column opposite faces, based on AISC [16]. The subassemblies are extracted from interior joints of moment frames, deflected under lateral loads. In moment frames the inflection points are formed near the mid-span of beams and mid-height of columns. By this assumption, the inflection points of moment frames are considered to be the ends of subassembly beams and columns with hinged supports.

The proportioning of specimens is governed by the maximum load capacity and the stroke of the actuator. The specimens are designed to satisfy the strong-column weak-beam criterion to ensure a plastic mechanism of the beam. As box-columns are used ordinarily for two-way moment frames in Iran, and regarding large torsional stiffness and strength of such columns, a box-section was selected to eliminate the relevant instabilities and failure modes as well as to focus more on the connection behavior.

In this study, to construct AW-RBS connections, the beam webs were removed by a hand cutting torch and ground by a hand grinder. Two L-shape sections, prepared by dividing a cold-formed box-section along its diameter, were applied in Specimen 1 and two standard hot-rolled angle sections in Specimen 2 as the corrugated webs. The AW-RBS connection details of both specimens are illustrated in Fig. 3. The specimens were fabricated by a commercial fabricator. A welding detail without web cope was considered, as shown in detail-a in Fig. 3 [20]. The beam flanges

**Table 1**  
Mechanical properties of steel coupons.

Test Specimen	Member	Coupon	Yield strength (Mpa)	Tensile strength (Mpa)	Elongation (%)
1 & 2	Beam (IPE 180)	Web	391.0	495.8	25.0
1 & 2	Beam (IPE 180)	Flange	316.5	446.3	27.0
1 & 2	Column (Built-up 200 × 160 × 10)	Web & Flange Plates	253.0	370.0	41.0
1 & 2	Column (Built-up 200 × 160 × 10)	Panel zone & continuity plates	244.2	374.3	30.1
1	Corrugated plate (Cold-formed 50 × 50 × 3.5)	Side	406.0	449.0	18.0
2	Corrugated plate (Hot-rolled L50 × 50 × 4)	Leg	289.8	422.1	28.4

were connected to the column face by applying a prequalified CJP groove welding detail without backing bar with a root pass and a reinforcing fillet. The welds tabs were adopted in order to provide sound welding quality and they were removed after welding. CJP groove welds were applied between the continuity plates and the box-column, while steel backing bars were left in place. The beam webs were connected to the column face in both specimens by fillet welding. It should be mentioned that the implementation of a fillet weld in connecting the beam web to the column face seems difficult in the field welded connections because of fit-up tolerances. All groove welds were ultrasonically checked and all fillet welds were visually tested by a licensed inspector. The beams, columns, continuity plates and corrugated plates were all of A36 steel with nominal yield stress of 240 Mpa. The mechanical properties of steel coupons, obtained from the plates and sections of the specimens, are presented in Table 1, in accordance with ASTM A370 standard for tensile testing of the steel.

### 3.2. Design procedure of AW-RBS connections

The design procedure of AW-RBS connections is based on AISC seismic provisions [16]. The geometric design parameters are the distance from the column face to the start (parameter  $a$ ) and to the center of the corrugated region (parameter  $e$ ), as shown in Fig. 4. These design parameters are selected in accordance with AISC recommendations for radius cut RBS connections in order to obtain sensible trial values [21]. Accordingly, the distance to the reduced region ( $a$ ) is 50%–75% of the beam flange width ( $b_f$ ) and the reduced region length ( $b$ ) is 65%–85% of the beam depth ( $d_b$ ). The acceptable ranges of parameters  $a$  and  $e$  ( $e = a + b/2$ ), based on the above values, are as follows:

$$0.5b_f \leq a \leq 0.75b_f \quad (1)$$

$$(0.5b_f + 0.325d_b) \leq e \leq (0.75b_f + 0.425d_b). \quad (2)$$

According to Eqs. (1) and (2), the parameters  $a$  and  $e$  are 67.5 mm and 100 mm, respectively, in both specimens.

At the column face, the maximum moment should be smaller than the plastic moment of the beam in order to limit the possibility of fracture in the beam flange groove weld or surrounding heat affected regions. As shown in Fig. 4, the maximum moment demand at the column face ( $M_f$ ) is calculated by projecting the maximum expected moment ( $M_{AW-RBS}$ ) developed at the center of reduced region to the column face as follows:

$$M_f = M_{AW-RBS}(L + e)/L \quad (3)$$

where  $L$  is the distance from the center of the reduced region to the point of inflection in the moment diagram. The maximum expected moment at the center of the reduced region, considering strain hardening, is as follows:

$$M_{AW-RBS} = 1.1Z_{AW-RBS}F_{ye} \quad (4)$$

where  $Z_{AW-RBS}$  is the plastic section modulus of the corrugated region. It is calculated upon flanges only due to the accordion effect of the corrugated web and is equal to  $2t_f b_f (d_b - t_f)$ , where  $t_f$  is the flange thickness. The expected yield strength,  $F_{ye}$ , is equal to

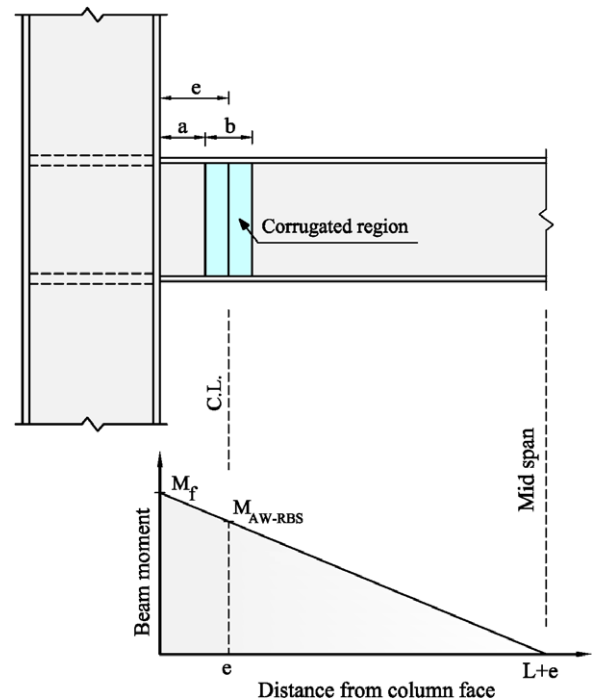


**Fig. 4.** Bending moment gradient for seismic loading.

$R_y F_y$ ; here,  $R_y$  is the difference between the minimum specified yield strength ( $F_y$ ) and the expected yield strength,  $R_y$ , of A36 steel hot-rolled structural shapes is 1.5, in accordance with AISC [16]. Moreover, the multiplier 1.1 accounts for the peak connection strength including limited strain hardening and other types of over-strength, proposed in AISC [16].

The ratio of the moment to the expected plastic moment capacity of the unreduced beam section at the column face ( $M_f/Z_b F_{ye}$ ) should be less than 1.0 to reduce the fracture vulnerability at beam flange groove welds; here,  $Z_b$  is the plastic section modulus of the unreduced beam section. This value is recommended to be 0.9 in practical design of radius cut RBS connections [22]. The other essential code provisions – such as shear capacity, panel zone, continuity plates and strong-column weak-beam requirements – should be controlled for plastic hinge demands.

In this study, test specimens were designed by implementing the proposed design procedure. The expected yield stress ( $F_{ye}$ ) was calculated based on a nominal yield stress of 240 Mpa and  $R_y$  factor of 1.5. The detailed design calculations for both test specimens are tabulated in Table 2.

As the conditions involved in the shear strength and stability of webs are changed in the corrugated region, the conventional formulation, proposed in AISC [16] for web shear, is not applicable. Therefore, the shear capacity and stability should be reinvestigated with respect to the shear behavior of corrugated plates.

The buckling failure of corrugated webs is mainly governed by interactive shear buckling as a result of the interaction between local and global buckling [23]. Eq. (5), presented by Driver et al. [24] for predicting the nominal shear strength ( $\tau_n$ ) of corrugated webs,

**Table 2**  
Design calculations for Test Specimens.

Test Specimen	$Z_{AW-RBS}$ ( $m^3 \times 10^{-6}$ )	$Z_b$ ( $m^3 \times 10^{-6}$ )	$M_{AW-RBS}$ (kN m)	$M_f$ (kN m)	$\frac{M_f}{Z_b F_y}$	$V_f$ (kN)	$\frac{V_f}{0.6A_w F_y}$	$V_{pz}$ (kN)	$R_v$ (kN)	$\frac{V_{pz}}{R_v}$	$\frac{\sum M_{pb}^*}{\sum M_{pc}^*}$
1 & 2	125	166	49.59	53.0	0.89	34.3	0.25	616.5	762.8	0.81	0.56

Shear at the column face:  $V_f = M_f / (L + e)$ , Web area at unreduced section:  $A_w$ ,

Panel zone shear demand:  $V_{pz} = 2M_f / (d_b - t_f)$ ,

Panel zone shear capacity:  $R_v = 0.6F_y d_c t_p$ , where  $d_c$  is the column depth and  $t_p$  is the thickness of the panel zone including both webs,

Bending moment in the beam and column at the intersection of beam and column centerlines:  $M_{pb}^*$  and  $M_{pc}^*$ .

is used to evaluate the lower bound strength of the interaction buckling failure mode as follows:

$$\tau_n = \sqrt{\frac{(\tau_{cr,L} \cdot \tau_{cr,G})^2}{\tau_{cr,L}^2 + \tau_{cr,G}^2}} \quad (5)$$

where  $\tau_{cr,L}$  and  $\tau_{cr,G}$  are the local and global shear buckling stress, respectively. According to the buckling stress value, local and global shear buckles could be both elastic and inelastic. If the elastic buckling stress,  $\tau_{cr,i}^E$ , is less than 80% of the shear yield stress,  $\tau_{cr,i}^E \leq 0.8\tau_y$  ( $i = L$ (Local),  $G$ (Global)), then the behavior is governed by elastic buckling and  $\tau_{cr,i}$  in Eq. (5) is assumed to be elastic ( $\tau_{cr,i} = \tau_{cr,i}^E$ ). Otherwise, inelastic buckling will occur and the buckling stress,  $\tau_{cr,i}$  in Eq. (5), is calculated as follows [17]:

$$\tau_{cr,i} = \sqrt{0.8\tau_y \tau_{cr,i}^E} \leq \tau_y, \quad i = L, G. \quad (6)$$

The shear yield stress ( $\tau_y$ ), based on Von Mises yield criterion, is

$$\tau_y = F_y / \sqrt{3}. \quad (7)$$

The elastic buckling stress of the corrugated web in local and global buckling,  $\tau_{cr,i}^E$  ( $i = L, G$ ), can be calculated based on the plate stability theory. The corrugated web sub-panels (Fig. 2) support each other along their vertical edges and the beam flanges support the horizontal edges (Fig. 3). Therefore, the elastic shear local buckling stress of a single sub-panel is [17]

$$\tau_{cr,L}^E = k_s \frac{\pi^2 E}{12(1 - \nu^2)(L_c/t_c)^2} \quad (8)$$

where

$k_s$  = the local shear buckling coefficient, a function of  $h_w/t_c$  and the boundary condition of the sub-panel;

$h_w$  = web height;

$t_c$  = thickness of each corrugated plate;

$\nu$  = Poisson's ratio;

$E$  = the Young's modulus;

$L_c$  = the sub-panel width, see Fig. 2.

The global buckling of each L-shaped corrugated plate can be conservatively calculated based on the buckling formulation of orthotropic plates in shear, assuming that each L-shaped plate is supported by the other one along the vertical edge and by beam flanges along the top and bottom edges. According to Sayed-Ahmed [25], the elastic shear global buckling of zigzag corrugated webs is calculated by Eqs. (9)–(11).

$$\tau_{cr,G}^E = k_g \frac{(D_y D_x^3)^{1/4}}{h_w^2 t_c} \quad (9)$$

$$D_x = \cos \theta \left( \frac{E t_c^3}{12} \right) \quad (10)$$

$$D_y = \frac{E}{d} \left( \frac{t_c (d \tan \theta)^3}{12 \sin \theta} \right) \quad (11)$$

where

$k_g$  = the global shear buckling coefficient, mainly depending on the web top and bottom boundary conditions;

$D_x$  &  $D_y$  = flexural rigidities of orthotropic plates;

$$d = L_c \cos \theta;$$

$\theta$  = corrugation angle, as defined in Fig. 2.

The elastic shear global buckling stress is summarized, substituting Eqs. (10) and (11) for Eq. (9), as

$$\tau_{cr,G}^E = k_g \frac{E \sqrt{\sin^3 \theta / \cos \theta}}{12} \left( \frac{t_c}{h_w} \right)^2 \left( \frac{L_c}{t_c} \right)^{1.5}. \quad (12)$$

The parameters  $L_c/t_c$  and  $h_w/t_c$  should be determined assuming  $\tau_{cr,L} = \tau_y$  and  $\tau_{cr,G} = \tau_y$  in order to avoid local and global buckling within the corrugated region and to satisfy the maximum shear strength of corrugated web. Hence, if  $\nu = 0.3$ ,  $\theta = 45^\circ$ ,  $k_s = 5.34$  (long sub-panel with simply supported edges) and  $k_g = 31.6$  (panel with simply supported edges) then  $L_c/t_c$  and  $h_w/t_c$  are as follows:

$$\frac{L_c}{t_c} \leq 2.586 \sqrt{\frac{E}{F_y}} \quad (13)$$

$$\frac{h_w}{t_c} \leq \sqrt{2.58 \frac{E}{F_y} \left( \frac{L_c}{t_c} \right)^{1.5}}. \quad (14)$$

It should be mentioned that the  $k_s$  and  $k_g$  values are selected conservatively [25]. According to Eq. (5), the maximum nominal capacity of a corrugated web ( $\tau_n^{\max}$ ) is calculated by the following formula, regarding the above-mentioned limitations of  $L_c/t_c$  and  $h_w/t_c$ , which ensure shear yielding in local and global buckling ( $\tau_{cr,i} = \tau_y$ ):

$$\tau_n^{\max} = \frac{\tau_y}{\sqrt{2}}. \quad (15)$$

According to Eq. (15), the thickness of the corrugated web  $t_c$  (thickness of each corrugated plate) should be at least  $t_w / \sqrt{2}$  in order to have equal shear strength both inside and outside the corrugated region; here,  $t_w$  is the flat web thickness. The shear design of the corrugated web in both specimens is summarized in Table 3.

### 3.3. Test setup

In this study, the tests were conducted in the structural laboratory of the University of Tehran. The test setup was designed to provide expected boundary conditions for the subassemblies. The column base was attached to the strong floor by a hinged connection and the beam ends were supported by adjustable ones with lateral movement capability to provide the roller boundary condition.

A hydraulic actuator with 100 kN capacity and  $\pm 200$  mm stroke was used for applying cyclic horizontal displacements to the top of the column. The two ends of the actuator were connected to the specimen and the rigid frame by a free-to-rotate ball and socket connection to simulate the pinned end boundary condition. The lateral supports were provided by applying two external frames for each beam and another one near the loading point for the column in order to avoid out-of-plane movement of the specimen, lateral-torsional buckling of beams, column rotation, and local instabilities at the loading point. The test setup configuration and overall dimensions of the specimens are shown in Fig. 5.

**Table 3**  
Shear design of corrugated plates.

Test Specimen	$V_{corr}$ (kN)	$\tau_{corr}$ (MPa)	$\frac{L_c}{t_c} / 2.586 \sqrt{\frac{E}{F_y}}$	$\frac{h_{av}}{t_c} / \sqrt{2.58 \frac{E}{F_y} \left(\frac{L_c}{t_c}\right)^{1.5}}$	$\tau_n$ (Mpa)	$\tau_{corr} / \tau_n$
1	33.7	29.3	0.19	0.14	99.9	0.29
2	33.7	25.7	0.17	0.13	99.9	0.26

Shear demand at the center of corrugated region:  $V_{corr} = M_f / L$ ,

Shear stress of the corrugated plates:  $\tau_{corr} = V_{corr} / (2A_{corr})$ ,

Shear area of each L-shaped corrugated plate:  $A_{corr} = (d_b - 2t_f) \times t_c$ .

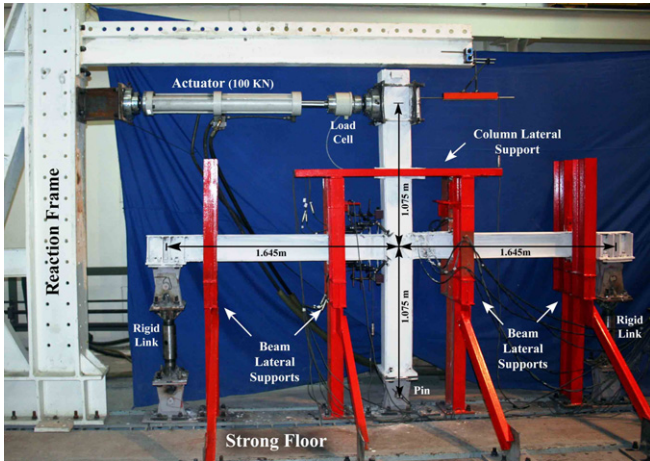


**Fig. 5.** Test setup configuration and overall dimensions of the specimens (photograph of Test Specimen 1).

### 3.4. Loading history, testing method and instrumentation

In this research, the specimens were tested by imposing a prescribed quasi-static cyclic displacement specified in the AISC seismic provision [16]. The total story drift angle was calculated by dividing the exerted displacement by the column height. The loading history was of six cycles, each of 0.375%, 0.5%, and 0.75% total story drift angle, sequentially. The next four cycles were at 1% story drift, followed by two cycles each of successive increasing drift percentages (i.e., 2, 3, 4...%). The cyclic tests were accomplished with a low rate for best monitoring the responses of the specimens as well as their deformations during the loading history.

Each specimen was equipped with LVDTs and strain gages. Six LVDTs were applied for monitoring the plastic hinge rotation and two other inclined ones for recording panel zone shear deformations. Several strain gages were pasted on the beam flange, beam web, corrugated plates and panel zone in order to measure the history of strains in the specimens. The instrumentation scheme is shown in Fig. 6.

The horizontal displacement of the actuator was measured by its internal displacement transducer and also by an external LVDT. The applied loads were measured by the load cell installed between the actuator and the specimen, as shown in Fig. 5. The data sent from the LVDTs and the strain gages were recorded using a digital data logger.

## 4. The experimental results

Global and local seismic behaviors of the specimens are presented herein by means of test observations and also analyses of instrumentation records. These investigations are used to verify the performance of the AW-RBS connection and the proposed design method.

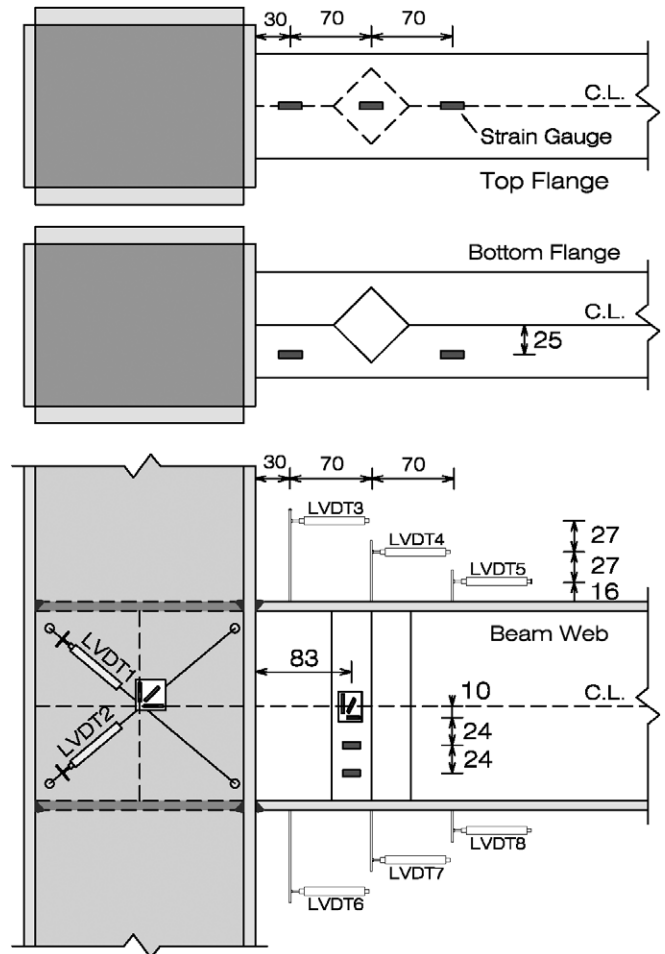


**Fig. 6.** The location of pasted strain gages and the LVDTs installed on the specimens (all dimensions are in mm).

### 4.1. Test observations

#### 4.1.1. Observations of Test Specimen 1

The first yielding of Test Specimen 1 emerged after minor flaking of the whitewash coating of both beam flanges at the center of the corrugated region during the first cycle of 1.5% story drift cycles. The yielding was more apparent after 2% story drift cycles. It was spread over the entire reduced region during 3% story drift, while no sign of yielding was observed in the corrugated web and the beam outside the reduced region. The flange yielding was extended toward the column face and beam end during the first cycle of 4% story drift; minor flaking of the whitewash was observed near CJP welds in the second cycle. The yielding patterns continued during 5% and 6% story drift cycles; the yielding was more extended to both sides of the corrugated region and it became nearly apparent outside the corrugated region, near the column face. In addition, a minor flaking of the whitewash was observed at the corrugated web corner near the left beam flange. Here, a

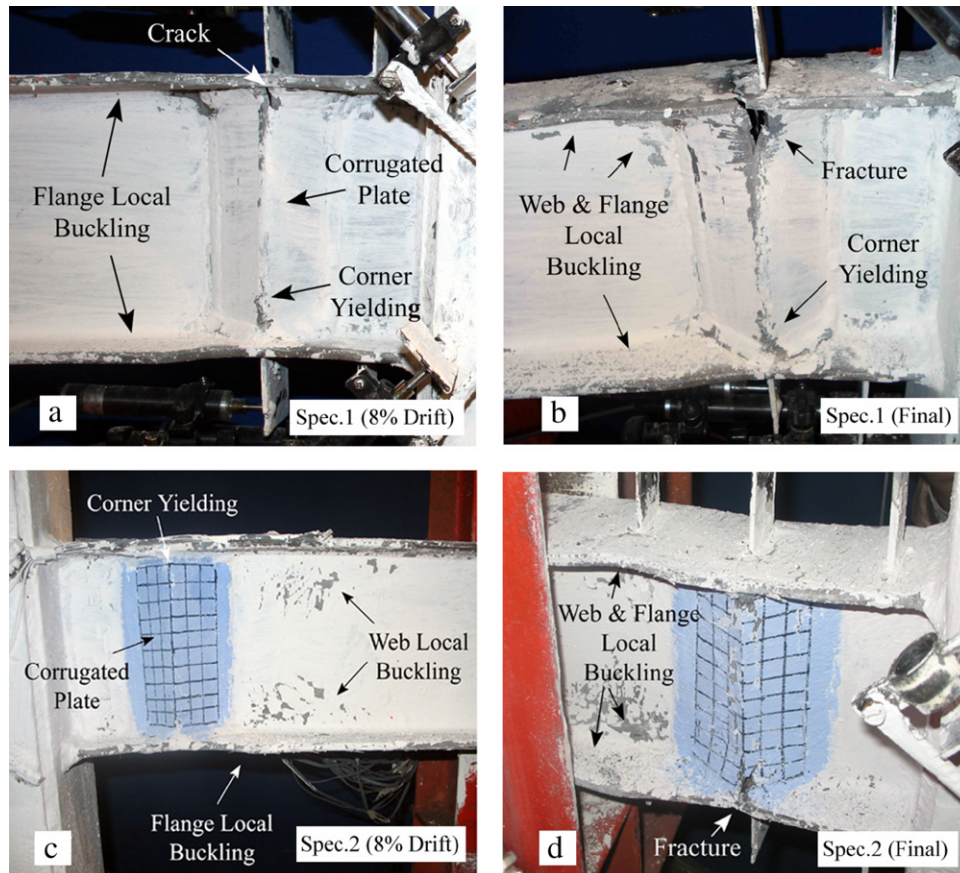


Fig. 7. Test Specimen 1. (a): 8% story drift (first cycle); (b) at the end (9% story drift). Test Specimen 2. (c): 8% story drift (last cycle); (d) at the end (9% story drift).

flange local buckling was detected before the corrugated region in both beams following the first cycle of 7% story drift. Furthermore, a lateral flange movement commenced at the end of the second cycle in the right beam; this was followed by the onset of the beam web buckling, although its amplitudes were very small. The amplitude of buckling increased in the first cycle of 8% story drift and during the second cycle. The yielding at the corrugated web corners extended into the beam depth on both sides of the specimen as well as the connection line of the corrugated plates to the flat web. In addition, the cracks were initiated in the fillet welds at each corner of the left beam corrugated web; subsequently, low cycle fatigue cracks were formed in the base metal at the corners, as shown in Fig. 7(a). The cracks extended down into the corrugated plate and became more extensive during the first cycle of 9% story drift. Finally, the test was terminated due to the fractures in the web and in the top flange of the left beam, as shown in Fig. 7(b).

#### 4.1.2. Observations of Test Specimen 2

During the first cycle of 1.5% story drift, the yielding initiated in the beam flanges after a minor flaking within the corrugated region and extended to the entire reduced region at the end of 2% story drift. During 3% story drift cycles, the yielding of the reduced region was followed by a minor yielding outside the reduced region near the column face, and also before the reduced region. During 4% and 5% story drift cycles, the yielding of beam flanges extended about 25 cm from the column face towards the beam end before the corrugated region and then slightly towards the flat web. In the last cycle of 5% story drift, it became extensive adjacent to the CJP welds. In the first cycle of 6% story drift, a minor flaking was detected at the corrugated web corner, near the beam flange. During 6% story drift cycles, the flange local buckling commenced outside the corrugated region; this was then followed by web local

buckling in both beams despite very small amplitude of buckles. At the end of the 8% story drift cycles, the amplitudes of the flange and web buckles became more extensive and the right beam top flange moved laterally, while it was in compression. Moreover, the yielding pattern continued to spread into the beam web adjacent to the column face, as shown in Fig. 7(c).

In the first cycle of 9% story drift, the flange and web buckles grew rapidly and the flange lateral movement became extensive. During the second cycle, cracks were found in the fillet welds at the corners of the corrugated plates near the left beam bottom flange. The yielding extended to the corners of the corrugated plates throughout the beam depth. It also extended along the connection line of corrugated plates to the flat web. The test was continued with 9% story drift cycles to investigate the failure modes because of actuator stroke limitation. In the first cycle, low cycle fatigue cracks were formed at the corners of the corrugated web base metal and in the second cycle they propagated across the entire beam bottom flange. The cracks resulted in a ductile fracture and the test was terminated immediately at this point, as shown in Fig. 7(d).

#### 4.2. Investigation of the general behavior

The column tip load versus column tip displacement and total story drift of both specimens are shown in the Fig. 8(a) & (b). The total story drift was calculated by dividing the column tip displacement by the distance from the column base to the centerline of the actuator. Both specimens showed quite stable inelastic behaviors and favorable energy dissipation capacities throughout testing. The connection performance exceeded the AISC seismic provision requirements because only a minor degradation was observed during the last cycles of loading due to

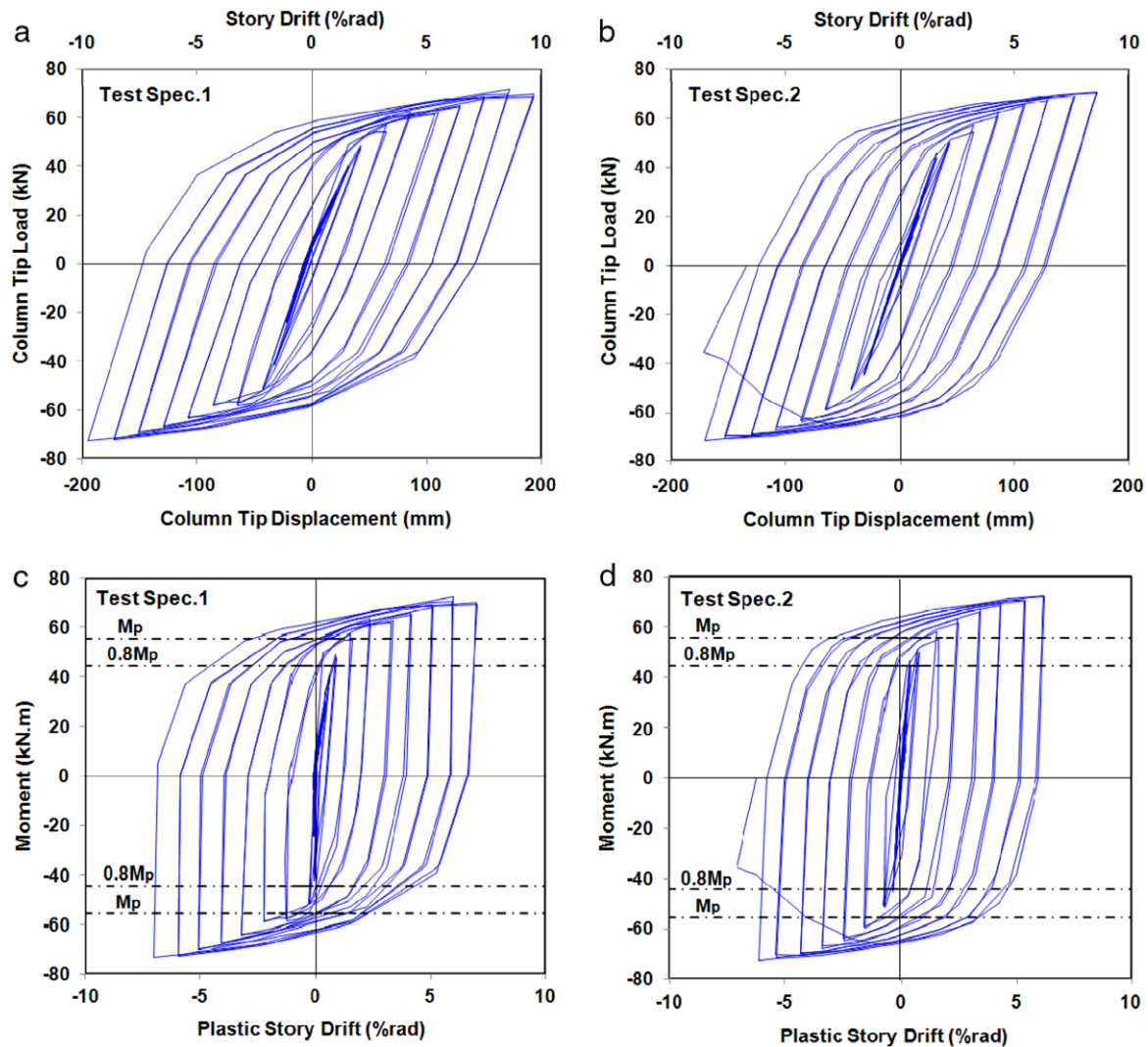


Fig. 8. (a) and (b): Load versus column tip displacement (and story drift angle); (c) and (d): Moment at the column face versus plastic rotation.

the beam flange and web buckles. It should be mentioned that this provision accepts the maximum of 20% strength degradation until 4% total story drift for qualifying a connection for special moment resisting frames [16]. The proposed connection also met FEMA-350 criteria as the test specimens resisted up to 9% story drift. The mentioned criteria require total rotation of 4% story drift before any significant strength degradation and 6% story drift before losing the total resistance [14].

The moment at the column face versus total plastic rotation of the specimens are shown in Fig. 8(c) and (d). According to the figures, at least 7% total plastic rotation was provided by the specimens without any significant strength degradation. This was more than twice the required 3% plastic story drift for special moment frames in the previous version of AISC seismic provisions [26].

#### 4.3. Investigation of the plastic hinge behavior

The effectiveness of the proposed connection in reducing the beam's plastic moment capacity is examined by using the test results. The beam moment backbone curves at the plastic hinge location (reduced region) during the test cycles for both specimens are shown Fig. 9. According to the backbone curves, the plastic moment is estimated to be about 43.5 kN m in the reduced region. The plastic moment of the beam full section is about 55.6 kN m,

based on the beam's plastic section modulus ( $Z_b$ ) and distinct values of real yield stress on flange and web materials (as reported in Table 1). While the  $Z_{AW-RBS}$  to  $Z_b$  ratio is 0.75, that of the reduced section to full section plastic moment is 0.78. This difference is explained by the effect of the corrugated web on the plastic modulus of the reduced region. Therefore, the web contribution to the plastic moment capacity is dramatically reduced due to the accordion effect of the corrugated plates and the plastic hinge formed in the reduced region of the beam far from the column face. Furthermore, the plastic moment of the reduced section is reasonably estimated at the corrugated region by the proposed design method.

The development of a reduced region and the concentration of plastic strains, in this region were observed through the tests and recorded by means of pasted strain gages. Fig. 10 shows the envelope of vertical profile of axial strain in the plastic hinge in the corrugated web and beam flange for both specimens. According to this figure, the top flange strains are substituted for the bottom ones at the reduced region center, assuming the top and bottom flange strains to be nearly equal. As seen in the figure, the axial stress is negligible along the beam axis in the corrugated web compared to the flange strains excepted for web areas near the beam flange because of the local effects of the beam flanges.

Regarding the observations, the general behaviors of both specimens were nearly similar. However, the cold-formed corrugated

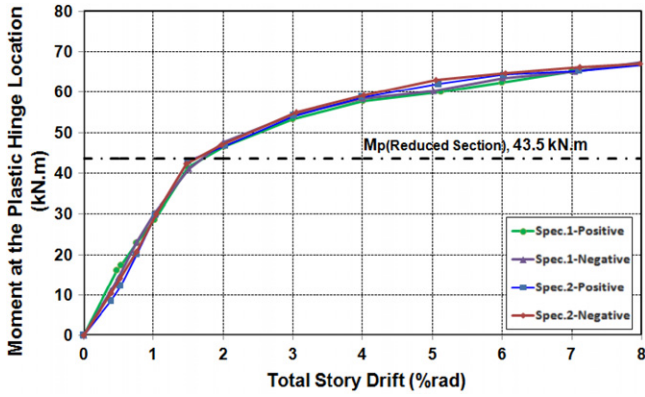


Fig. 9. Backbone curve of the beam moment at the plastic hinge location (reduce region).

section used in Test Specimen 1 showed more brittle behavior near the corners compared to the hot-rolled angle section in Test Specimen 2. In cold-formed sections, the material is nearly non-ductile as they experience high residual plastic strains during the cold rolling at the round corners. Moreover, in the corrugated region, the initiation of low cyclic fatigue cracks is accelerated by high ductility demands due to the large plastic rotations at the corners. Therefore, the material of the cold-formed section is expected to have lower ductility, as seen in the tests.

The formation of a plastic hinge at the reduced section can also be demonstrated by means of a longitudinal strain profile along the beam top flange, as shown in Fig. 11. The formation of the plastic hinge in the predefined region is confirmed by higher values of normalized strain, developed in the flanges within the reduced section. According to Fig. 11, the strain values at the reduced section are over three times the strains near the column face. The demand of plastic strains is decreased near the column face, and therefore the possibility of fracture is reduced at the beam-to-column CJP welds due to the concentration of plastic strains within the reduced region. According to the curves, the first yielding in the plastic hinge is in 1–1.5% story drift cycles in both specimens; the normalized strain is about 22 and 15 at 4% story drift in Test Specimens 1 and 2, respectively. Therefore, plastic hinges are completely formed in both specimens at the end of 4% story drift. It should be noted that the inherent flange and web local buckling potential are eliminated at the plastic hinge location by means of the corrugated web, and the buckles occur before the

corrugated region, as seen during the final cycles of the test. The width-to-thickness ratio of the flanges decreases because of the corrugated web at the plastic hinge and consequently the buckling load of the beam flanges increases.

#### 4.4. Investigating the panel zone behavior

The shear deformation of the panel zone was measured using external inclined LVDTs and a rosette strain gage, pasted on the center of the panel zone, as illustrated in Fig. 6. The results of diagonal deformations within the panel zone were converted into the story drift portion of the panel. The maximum story drifts developed by the panel zone deformation were about 0.42% and 0.35% story drift in Test Specimens 1 and 2, respectively. The maximum average shear deformation within the panel zone area was estimated to be twice the yield shear strain of the panel zone. Additionally, the envelope values of normalized Von Mises strain calculated from the measurements of rosette strain gage showed that the yielding in the panel zone was first initiated at the end of 2% story drift, and the normalized Von Mises strain was about 2.5 at 6% story drift.

The above results from the rosette gage are in close agreement with the panel zone average shear deformation, obtained by diagonal LVDTs. Since no type of instability or flaking of the whitewash coating was observed in the panel zone of both specimens at the final stage of cyclic loading, the panel zone balanced behavior is assumed adequate and reliable.

### 5. Analytical study of the connection behavior

The connection's cyclic behavior has been investigated numerically after being calibrated by the experimental results for better understanding of the seismic behavior of the new proposed connection. The cyclic response, the plastification pattern, the behavior of the reduced region and other components of the connection are analyzed and compared with the test results.

#### 5.1. Finite element modeling

Both specimens were three-dimensionally modeled by the general purpose finite element program ANSYS [27]. In this regard the shells elements were used for modeling in order to achieve a computationally efficient model. The geometry of finite element models, including member section sizes, all dimensions

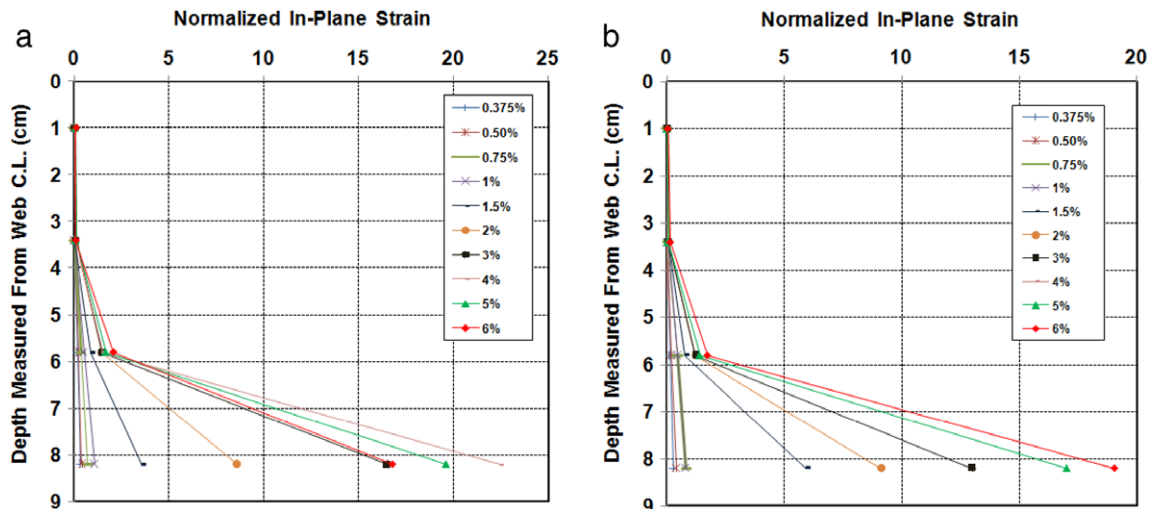


Fig. 10. The vertical profile envelope of axial strain through the corrugated region: (a) Test Specimen 1; (b) Test Specimen 2.

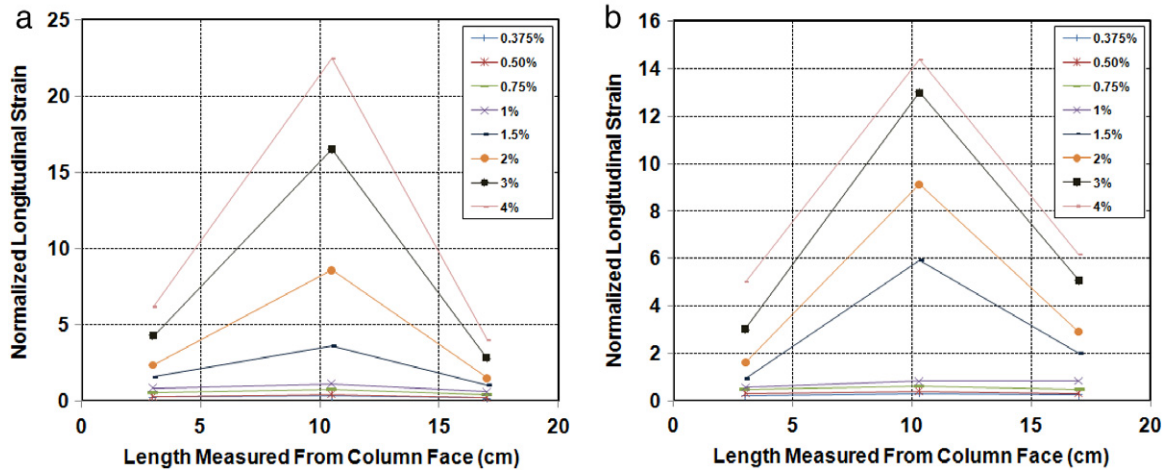


Fig. 11. Normalized longitudinal strain profile along the beam top flange: (a) Test Specimen 1; (b) Test Specimen 2. (The strains are not shown due to a strain gage malfunction after 4% story drift.)

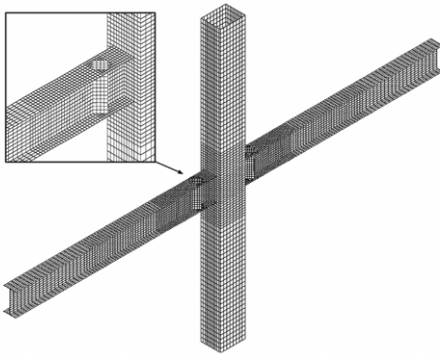


Fig. 12. Finite element model of Test Specimen 1.

and boundary conditions, were considered as per the subassembly used in the experimental program. Here, a quadrilateral four-node shell element (SHELL43 element) with plasticity, large deflection and large strain capability was used. A relatively finer mesh was applied therein based on the sharp stress gradient around the corrugated region in the beam and around the panel zone in the column. While it was assumed that the connected parts were completely joined together by the welds, neither complete joint penetration welds nor fillet welds were explicitly modeled. The out-of-plane movement of the beam flange was restrained near the plastic hinges and beam ends in accordance with the lateral bracing of test specimens in order to avoid global instabilities. Additionally, the column was laterally supported at the base and at the loading point. The overall view of the finite element model of Test Specimen 1 is shown in Fig. 12.

### 5.2. Finite element analysis

Regarding the geometric nonlinearities, expected in the model, a geometric imperfection was imposed on the mesh with the distribution similar to the first eigenvector, resulting from the eigen buckling analysis of the connection. A tri-linear stress-strain curve was used to represent the material properties. The Von Mises yield criterion and kinematic hardening rule were adopted to consider the plasticity behavior. The yield strength ( $F_y$ ) and the ultimate strength ( $F_u$ ) of the materials were considered as per the tensile coupon test results, as summarized in Table 1. The Young's modulus of elasticity, tangent modulus and Poisson's ratio were assumed as 203 Gpa, 0.03 Young's modulus and 0.3, respectively, for all materials of the analysis.

A cyclic displacement with increasing amplitude, similar to the experimental loading protocol, was incrementally imposed to the column tip. The cycles with amplitudes of less than 1% story drift were eliminated due to elastic behavior of the model.

### 5.3. Finite element results

The cyclic responses of the specimens, predicted analytically, are correlated suitably by experimental results for both specimens, as shown in Fig. 13. Here, the general validity of the finite element model used in this study is confirmed in predicting the cyclic behavior of the connection. No degradation is seen in the hysteretic responses of specimens throughout the finite element analysis. However, local buckling of the beam flange occurred during 6% story drift, leading to a decrease of the hardening slope and a flattening of the curve during the last cycles. Regarding the similar global behaviors of the Test Specimen models in the analytical study, the results are only presented for Test Specimen 1.

The deformed shape and the plastic strain distribution of Test Specimen 1 model are shown in Fig. 14 at 6% story drift. According to the results, plastic hinges are completely formed in the predefined reduced region, and the plastic deformations are concentrated therein. Furthermore, based on the analytical results, the plastic strains are about one fifth of the strain near the column face, resulting in the reduction of the vulnerability of CJP welds to probable fractures. The local plastic strains at the corners of the corrugated plates show brittle failure potential, as seen in the tests. Generally, the yielding and buckling patterns of the analytical model are in good agreement with the test results.

Additionally, the accordion effect of the corrugated plate is precisely studied by the finite element analysis. The vertical profile of longitudinal stresses in the corrugated region is presented in Fig. 15. The web's longitudinal stresses are much lower than the flange stresses within the corrugated region, excluding the areas adjacent to the flanges. Therefore, the effectiveness of the corrugated plates in reducing the web's contribution to the bending strength and stiffness of beam section is verified.

According to the analytical results, the connection plates, such as continuity plates, and the panel zones experience low levels of plastic strains and the inelastic deformation is mostly developed in the beam's plastic hinge. The maximum Von Mises strain, developed in the model at the panel zone, is about two times the yield strain at 6% story drift. This value shows a good agreement between the experimental and analytical results at the panel zone.

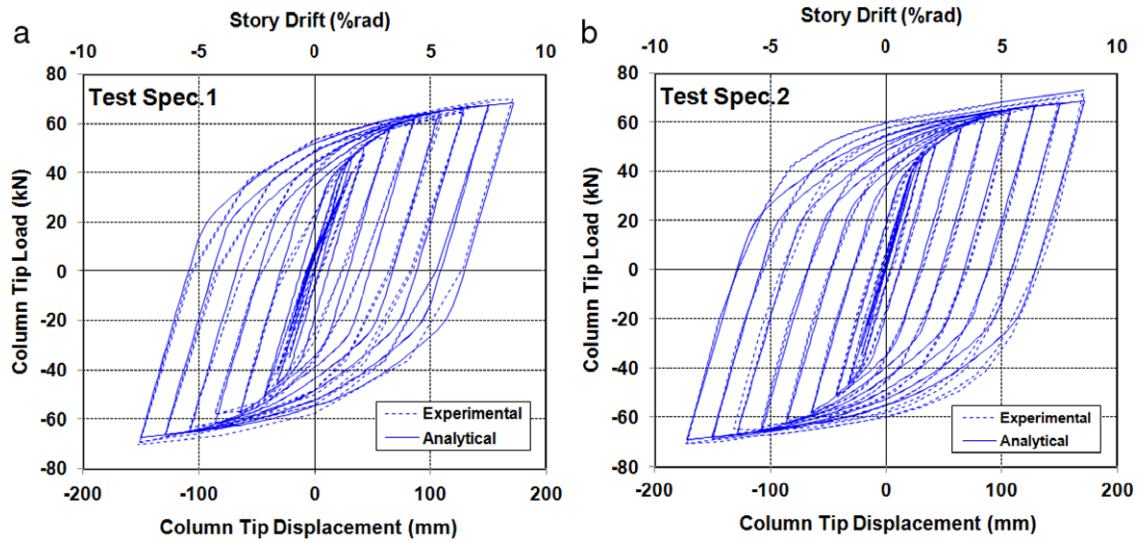


Fig. 13. Comparing the experimental cyclic responses to the finite element cyclic results. (a): Test Specimen 1; (b): Test Specimen 2.

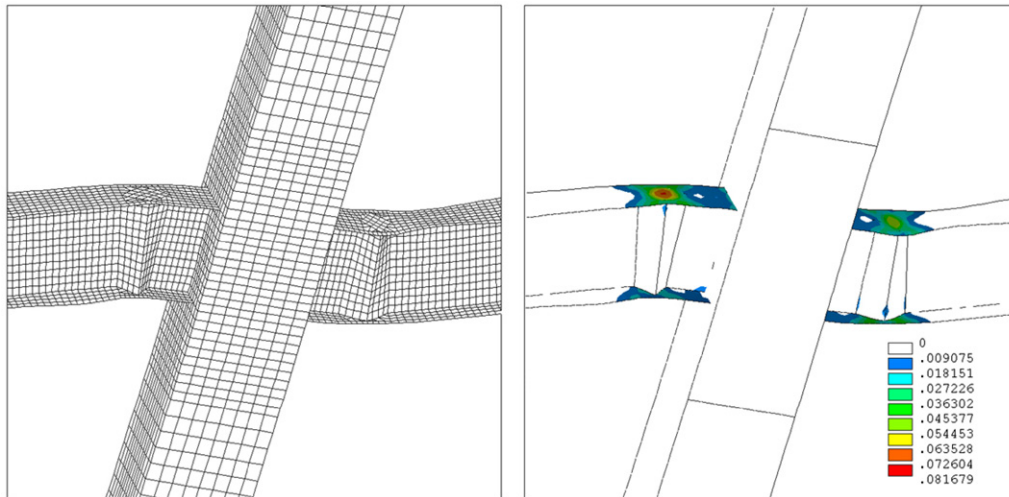


Fig. 14. Deformed shape and Von Mises plastic strain distribution in Test Specimen 1 at 6% story drift.

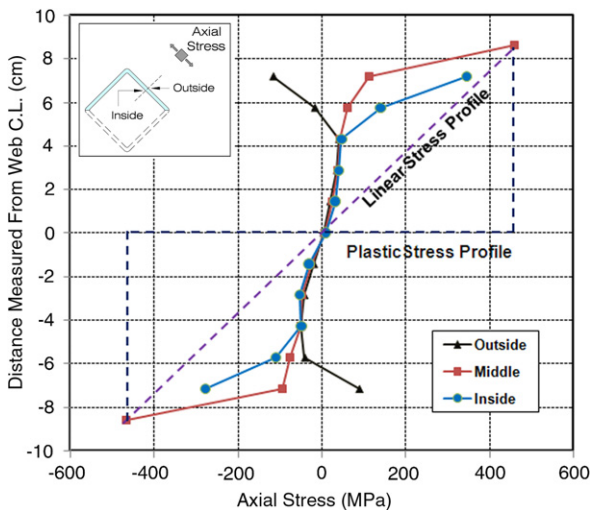


Fig. 15. The vertical profile of axial nodal stresses at the corrugated region in Test Specimen 1 at 6% story drift.

## 6. Conclusions

In this study, a new type of RBS connection, AW-RBS, developed by reducing the web contribution in the moment strength of the section, has been presented. According to the experimental and analytical results of two almost identical specimens, a plastic hinge is formed in the reduced region and the extensive yielding that occurs in this area is away from column face. There being no significant strength loss for more than 8% story drift angle in the cyclic tests shows that the nonlinear rotation capacity of the proposed connection is in excess of the current requirements for qualifying connections in special moment frames. In addition, the followings are concluded as per the presented experimental and analytical results:

- The connection can reduce the plastic strain demands near CJP welds and effectively concentrate the plastic strains within the reduced region. Accordingly, no fracture was observed outside the plastic hinge area in the tests.
- According to the experimental results, the plastic hinge capacity can be estimated in the corrugated region based on the beam flanges only and the contribution of the beam web to the plastic hinge capacity is negligible because of the web accordion behavior.

- As the occurrence of flange buckles is deferred by the corrugated plates, reliable and stable plastic hinge behavior is obtained.
- Cold-formed corrugated plates used in the plastic hinge area are found to have low ductility capacity, and therefore hot-rolled alternatives are recommended.
- According to the analytical and experimental results, the inelastic rotations are mostly provided by reliable and ductile plastic hinge rotation of the connection compared to those provided by connection plate deformations or panel zone deformations.

Despite the acceptable seismic performance of the designed connection, the results may not necessarily be extrapolated to the deeper beams used frequently in moment frame constructions. Therefore, further research is needed in identifying the connection behaviors in different sizes of beams and columns as well as different types of corrugated regions.

## References

- [1] Plumier A. The Dogbone: Back to the future. *Engineering Journal*, AISC 1997; 34(2):61–7. 2nd Quarter.
- [2] FEMA 355D. State of the art report on connection performance. Prepared by the SAC Joint Venture for the Federal Emergency Management Agency. Washington, DC; 2000.
- [3] Uang C-M, Chi B. Cyclic response and design recommendations of RBS moment connections with deep column. *J Struct Eng*, ASCE 2002;128(4):464–73.
- [4] Chi B, Uang C-M. Cyclic response and design recommendations of reduced beam section moment connections with deep columns. *J Struct Eng*, ASCE 2002;128(4):464–73.
- [5] Zhang X, Ricles J-M. Experimental evaluation of reduced beam section connections to deep columns. *J Struct Eng*, ASCE 2006;132(3):346–57.
- [6] Zhang X, Ricles J-M. Seismic behavior of reduced beam section moment connections to deep columns. *J Struct Eng*, ASCE 2006;132(3):558–67.
- [7] Lee C-H, Jeon S-W, Kim J-H, Uang C-M. Effects of panel zone strength and beam web connection method on seismic performance of reduced beam section steel moment connections. *J Struct Eng*, ASCE 2005;131(12):1854–65.
- [8] Nakashima M, Kanao I. Lateral instability and lateral bracing of steel beams subjected to cyclic loading. *J Struct Eng*, ASCE 2002;128(10):1308–16.
- [9] Uang C-M, Fan C-C. Cyclic stability criteria for steel moment connections with reduced beam section. *J Struct Eng*, ASCE 2001;127(9):1021–7.
- [10] Shen J, Kitjasetanphun T, Srivanich W. Seismic performance of steel moment frames with reduced beam sections. *Eng Struct* 2000;22:968–83.
- [11] Kitjasetanphun T, Shen J, Srivanich W, Hao H. Inelastic analysis of steel frames with reduced beam section. *Struct Design Tall Build* 2001;10:231–44.
- [12] Jin J, El-Tawil S. Seismic performance of steel frames with reduced beam section connections. *J Constr Steel Res* 2005;61:453–71.
- [13] Tremblay R, Filiatrault A. Seismic performance of steel moment resisting frames retrofitted with a locally reduced beam section connection. *Can J Civ Eng* 1997;24:78–89.
- [14] SAC. Seismic design criteria for new moment-resisting steel frame construction. Report no. FEMA 350, SAC Joint Venture, Sacramento, California; 2000.
- [15] Wilkinson S, Hurdman G, Crowther A. A moment resisting connection for earthquake resistant structures. *J Constr Steel Res* 2006;62:295–302.
- [16] AISC/ANSI 341-05. Seismic provisions for structural steel buildings. Chicago (IL): American Institute of Steel Construction, Inc.; 2005.
- [17] Elgaaly M, Seshadri A, Hamilton R-W. Bending strength of steel beams with corrugated webs. *J Struct Eng*, ASCE 1997;123(6):772–82.
- [18] Ezzeldin Yazeed S-A. Lateral torsion buckling of corrugated web steel girders. *Proc Inst Civ Eng Structures & Buildings* 2005;53–69.
- [19] Ibrahim S-I, El-Dakhkhni W-W, Elgaaly M. Behavior of bridge girders with corrugated webs under monotonic and cyclic loading. *Eng Struct* 2006;28:1941–55.
- [20] Gioncu V, Mazzolani F-M. Ductility of Seismic Resistant Steel Struct. 1st ed London: Spon Press, Taylor & Francis; 2002.
- [21] AISC/ANSI 358-05. Prequalified connections for special and intermediate steel moment frames for seismic applications specification. Chicago (IL): American Institute of Steel Construction, Inc.; 2005.
- [22] Engelhardt M-D, Winneberger T, Zekany A-J, Potyraj T-J. Experimental investigation of dogbone moment connections. *Eng J*, AISC 1998;128–39. Forth Quarter.
- [23] Yi J, Gil H, Youm K, Lee H. Interactive shear buckling behavior of trapezoidally corrugated steel webs. *Eng Struct* 2008;30:1659–66.
- [24] Driver R-G, Abbas H-H, Sause R. Shear behavior of corrugated web bridge girders. *J Struct Eng*, ASCE 2006;132:195–203.
- [25] Sayed-Ahmed Y-E. Behavior of steel and (or) composite girders with corrugated steel webs. *Can J Civ Eng* 2001;28:656–72.
- [26] American Institute of Steel Construction (AISC). Seismic provisions for structural steel buildings. Chicago (IL); 1997.
- [27] ANSYS (Revision 5.4). User's manual, theory, vol. IV. Swanson Analysis Systems, Inc; 1992.